Revised Manuscript for submission to *Journal of Membrane Science*

Osmotically enhanced reverse osmosis using hollow fiber membranes

Xianhui Li [a,b,c], Ying Mei [c,d], Junwei Zhang [c], Yang Yang [e], Lu Elfa Peng [c], Weihua Qing [c], Di He [a,b], Anthony G. Fane [f], Chuyang Y. Tang [c*]

[a] Key Laboratory for City Cluster Environmental Safety and Green Development of the Ministry of Education, Institute of Environmental and Ecological Engineering, Guangdong University of Technology, Guangzhou, 510006, P.R. China

[b] Southern Marine Science and Engineering Guangdong Laboratory (Guangzhou), Guangzhou, 511458, P.R. China

[c] Department of Civil Engineering, The University of Hong Kong, Pokfulam Road, Hong Kong S.A.R., P.R. China

[d] Research and Development Center for Watershed Environmental Eco-Engineering, Advanced Institute of Natural Sciences, Beijing Normal University, Zhuhai 519087, P.R. China

[e] Department of Chemical Engineering, Imperial College London, London SW7 2AZ, U.K.

[f] UNESCO Centre for Membrane Science and Technology, School of Chemical Engineering, University of New South Wales, Sydney, New South Wales, 2052, Australia

*Corresponding author: tangc@hku.hk

Abstract

Osmotically enhanced reverse osmosis (OERO) effectively increases the water recovery in desalination as it can reduce the transmembrane osmotic pressure by a sweep solution. Utilizing a model based on mass-transfer principles, we report the performance of a hollow-fiber RO membrane module in OERO as a function of the operating conditions, the fiber geometry, and the membrane properties. The hollow fiber system allows the feed and sweep solutions to flow on both sides of the membrane. To avoid energy-intensive solute/water separation, fertilizer can be employed as a "green" sweep solution as it can be directly used for fertigation (fertilized irrigation). Simulations indicated that the water recovery is significantly enhanced by increasing the water permeance and decreasing the structure parameter of the hollow fiber membranes. Further, an investigation into the role of feed salinity suggests that longer fibers can provide a higher water recovery in the case of low-salinity water reuse, while larger-diameter fibers achieve a more efficient seawater desalination. A single-stage OERO process facilitates the enhancement of water recovery from 35.5% and 14% to 36.5% and 34% in the case of low-salinity and high-salinity desalinations, respectively. This study provides theoretical perspectives into the design of hollow fiber modules for OERO processes.

Keywords: *Osmotically enhanced recovery, Mathematical model, Reverse osmosis membrane, Hollow fiber, Fertilizer*

1. Introduction

Reverse osmosis (RO) can turn the seawater and inland brackish water into fresh water. This has become the main approach to solve the global water shortage issue [1-3]. However, the practical application of RO desalination is constrained by a low water recovery and a relatively high energy consumption, as the process requires a considerable hydraulic pressure to overcome the osmotic pressure of the saline water (e.g. ~ 26 bar for 35 g L^{-1} seawater) for driving water molecules across membranes [4-5]. To address this issue, a concept known as "osmotically enhanced reverse osmosis" (OERO) has been reported, in which a solute (e.g. NaCl, Na_2SO_4, etc.) is added into the permeate side and is utilized as a sweep solution to counteract part of the feed osmotic pressure as depicted in **Fig. 1a** [6-8]. This system gives a higher water recovery than traditional RO processes under the same hydraulic pressure, thus a lower energy consumption for the RO step, which has been demonstrated in the treatment of highly saline water and shale gas wastewater [9-10].

A significant challenge in the OERO desalination process is the need to separate water from the diluted sweep solution, which consumes extra energy [11]. To avoid energy-intensive regeneration of the sweep solution, a feasible way is to select certain inorganic salts (e.g. KH_2PO_4, NH_4NO_3, KNO_3, etc.) as "green" solutes in the sweep solution such that the sweep solution, after being diluted, can be directly employed for fertigation (fertilized irrigation) [12-13]. This approach has been used previously in the context of fertilizer driven forward osmosis (FO) desalination for direct fertigation [14].

The second challenge for OERO is that the design of the membrane and the membrane modules are also of significant importance for realizing maximum performance. The spacer in the RO module induces membrane deformation at high hydraulic pressures, resulting in severe hydraulic pressure loss in the flow channel [15-17]. Therefore, compared with typical spiral-wound RO membranes, hollow fiber RO membranes provide several competitive advantages such as a lower hydraulic pressure loss, higher packing density and a larger effective surface area because of their mechanically self-supporting characteristics [18-19]. Most importantly, hollow fiber modules allow the feed and sweep solutions to flow on both sides of the membrane, which is a necessity for OERO but is currently not possible in typical spiral wound modules [20-22]. Although these studies confirm the advantages of hollow fiber membrane modules for achieving high-efficiency desalination of saline water, the technical feasibility and economics of utilizing fertilizer as sweep solution in the OERO system are still lacking. In addition, reducing the thickness of the support layer in hollow fiber membranes could effectively reduce the internal concentration polarization caused by the sweep solution [23]. Therefore, studying and understanding the impact of operating conditions and membrane modules on the OERO technique is critical for its future practical applications.

In this work, we establish a mathematical model based on mass-transfer principles to investigate the performance of hollow fiber membrane modules in an OERO process for applications in seawater desalination and water reuse. We study the influence of operating conditions (the operating pressure, the concentration, and the flow rates of the feed and sweep solutions), the fiber geometry (the fiber length and the fiber diameter) and membrane properties (the water permeance and the support structure) on water recovery and corresponding energy consumption. Moreover, experimental studies have been performed to support our simulation results. This research provides theoretical perspectives for in-depth understanding of sustainable fertigation by OERO technology and its membrane module design for practical applications.

2. Model development

2.1. Simulation of permeate flux in osmotically enhanced desalination process

In the OERO system, the sweep solution is in the fiber lumen and the feed solution is pressurized in the shell. The sweep and feed flows are counter-current and along axial directions to the fibers (**Fig. 1**). The derivation of the RO water and salt flux equations in an osmotically enhanced recovery desalination process is presented in the Supporting Information, **Section S1**. The derivation yields the following expressions for the water flux (J_w) and the salt flux (J_s):

$$J_w = A\left\{\Delta P - \frac{\pi_{f,b}\exp\left(\frac{J_w}{k}\right) - \pi_{s,b}\exp\left(-\frac{S}{D}J_w\right)}{1+\frac{B}{J_w}\left[\exp\left(\frac{J_w}{k}\right) - \exp\left(-\frac{S}{D}J_w\right)\right]}\right\} \tag{1}$$

$$J_s = B\left\{\frac{C_{f,b}\exp\left(\frac{J_w}{k}\right) - C_{s,b}\exp\left(-\frac{S}{D}J_w\right)}{1+\frac{B}{J_w}\left[\exp\left(\frac{J_w}{k}\right) - \exp\left(-\frac{S}{D}J_w\right)\right]}\right\} \tag{2}$$

where ΔP is the applied hydraulic pressure, k is the feed salt mass transfer coefficient in the shell side, S is the structure parameter of the membrane and D is the bulk diffusion coefficient of the salt. The terms $\exp(J_w/k)$ and $\exp(J_wS/D)$ are the moduli of the external concentration polarization (ECP) and the internal concentration polarization (ICP), respectively. A and B are the permeability coefficients of water and salt, respectively. $C_{f,b}$ and $C_{s,b}$ are the respective bulk solute concentrations of the feed and sweep. $\pi_{f,b}$ and $\pi_{s,b}$ are the bulk osmotic pressures for the feed and sweep, respectively. The osmotic pressure (π) is able to be expressed by the Van't Hoff equation.

$$\pi = \varphi iCRT \tag{3}$$

where i stands for the number of dissociating species, C represents the concentration of solute, T represents the temperature, R is the gas constant, and φ represents the osmotic coefficient.

In the OERO system, the outside-in hollow fiber membranes with small diameter are preferred due to their high pressure tolerance and low fouling tendency [21]. The pressure drop (P_i) inside the hollow fiber membrane thus cannot be ignored and is expressed by the Hagen-Poiseuille equation,

$$\frac{P_i}{dz} = \frac{32\mu v_i}{d_i^2} \tag{4}$$

where d_i is the inner diameter of the fiber, and v_i is the flow velocity inside the pore.

The pressure drop in the shell can be calculated from the empirical Ergun equation [24],

$$\frac{dP_S}{dz} = -\left\{\frac{150(1-\varepsilon)^2\mu v_S}{\varepsilon^3 d_p^2} + \frac{1.75(1-\varepsilon)\rho(v_S)^2}{\varepsilon^3 d_p}\right\} \tag{5}$$

where d_p is the characteristic diameter used in the equation and is defined as $1.5d_o$ for cylindrical fibers [25], and v_s is the velocity of flow in the shell.

Mass transfer coefficient k is calculated from Schmidt (S_c), Reynolds (R_e) and Sherwood (S_h) numbers with the equation,

$$k = \frac{S_h}{d_h} D \tag{6}$$

$$\mathrm{Re} = \frac{d_h v \rho}{\mu} \tag{7}$$

$$S_C = \frac{\mu}{\rho D} \tag{8}$$

where d_h is the hydraulic diameter. Therefore, it is necessary to calculate the Sherwood number and the hydraulic diameter for the shell side.

For the Sherwood number, when the flow is turbulent ($2300 < \mathrm{Re} \le 10^6$) [26],

$$S_h = 0.021 \left(\frac{1}{\sqrt{1-\varepsilon}} \right)^{0.45} \mathrm{Re}^{0.8} \, Sc^{0.33} \tag{9}$$

when the flow is laminar ($\mathrm{Re} \le 2300$) [26],

$$S_{h1} = 3.66 + 1.2 \left(\sqrt{1-\varepsilon} \right)^{-0.8} \tag{10}$$

$$S_{h2} = 1.165 \left(1 + 0.14 \left(\sqrt{1-\varepsilon} \right)^{-0.5} \right) \sqrt[3]{\frac{\mathrm{Re} \cdot Sc \cdot d_h}{l_{mem}}} \tag{11}$$

$$S_{h3} = \left(\frac{2}{1+22Sc} \right)^{1/6} \left(\frac{\mathrm{Re} \cdot Sc \cdot d_h}{l_{mem}} \right)^{1/2} \tag{12}$$

$$S_h = \left(S_{h1}^3 + S_{h2}^3 + S_{h3}^3 \right)^{1/3} \tag{13}$$

where l_{mem} is the length of the membrane and ε is the void fraction in the shell. The void fraction largely depends on the assignment of the hollow fibers and it is assumed that each fiber is a hexagon which is comprised with two components including a fiber channel and a shell (**Fig. 1**). Hence, the void fraction is defined as

$$\varepsilon = 1 - \frac{A_{fiber}}{A_{hexagon}} = 1 - \frac{\pi}{2\sqrt{3}} \frac{1}{\left(1 + \frac{f_d}{d_o} \right)^2} \tag{14}$$

where A_{fiber} is the occupied area of fiber, $A_{hexagon}$ is the catchment area of fiber, f_d is the distance between two fibers and is set constant as presented in **Table 1**, and d_o is the outer diameter of the fiber.

For the hydraulic diameter of the shell side, it is defined as

$$d_h = \frac{4A_{flow}}{P_{fiber}} \tag{15}$$

where A_{flow} is the cross sectional flow area in the fiber lumen, and P_{fiber} is the perimeter of circular cross section of the fiber.

Therefore,

$$d_h = \frac{4\left[2\sqrt{3}\left(\frac{d_o}{2}+\frac{f_o}{2}\right)^2 - \frac{\pi}{4}d_o^2\right]}{\pi d_o} = \frac{2\sqrt{3}\left(d_o + f_o\right)^2}{\pi d_o} - d_o \tag{16}$$

The NaCl solution was used as feed solution. The density (ρ_{NaCl}), viscosity (μ_{NaCl}) and diffusivity (D_{NaCl}) of NaCl solution are affected by solute concentration C, and they can be expressed by Eq. (17)-(19), respectively [27-28]:

$$\rho_{NaCl} = \left(0.0369C_{NaCl} + 1.0006\right) \times 1000 \tag{17}$$

$$\mu_{NaCl} = \left(0.0133{C_{NaCl}}^2 + 0.0734C_{NaCl} + 1.003\right)/1000 \tag{18}$$

$$D_{NaCl} = 0.0005{C_{NaCl}}^4 - 0.0088{C_{NaCl}}^3 + 0.0447{C_{NaCl}}^2 - 0.045C_{NaCl} + 1.489 \tag{19}$$

For simulation purpose, the fertilizer KH_2PO_4 was used as sweep solution. The density (ρ_{KH2PO4}), viscosity (μ_{KH2PO4}) and diffusivity (D_{KH2PO4}) of KH_2PO_4 solution are affected by solute concentration C, and they can be expressed by Eq. (20)-(22), respectively [29-30]:

$$\rho_{KH2PO4} = 8.8479 \times C_{KH2PO4}^2 + 110.17 \times C_{KH2PO4} + 1001.4 \tag{20}$$

$$\mu_{KH2PO4} = 0.0738 \times C_{KH2PO4}^3 - 0.0356 \times C_{KH2PO4}^2 + 0.2147 \times C_{KH2PO4} + 1.0035 \tag{21}$$

$$D_{KH2PO4} = -8.161 \times {C_{KH2PO4}}^{0.5} + 12.761C_{KH2PO4} - 14.996 \times {C_{KH2PO4}}^{1.5} + 5.683 \times C_{KH2PO4}^2 \tag{22}$$

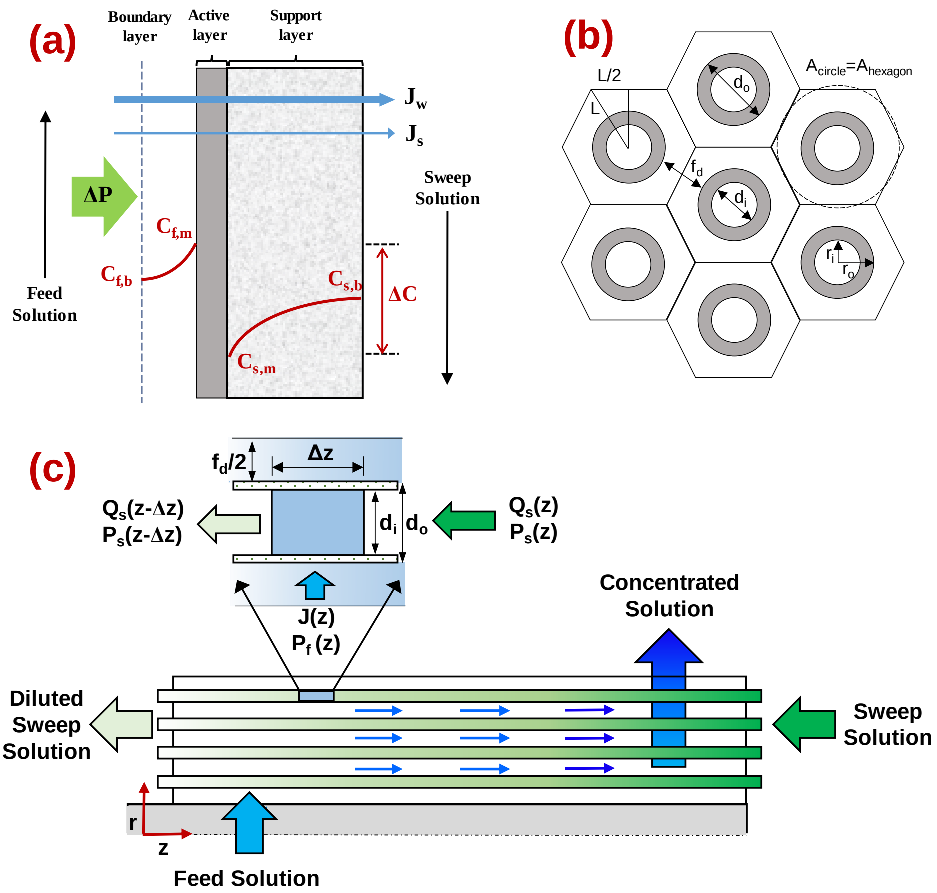

Fig. 1. Illustration of osmotically enhanced reverse osmosis (OERO) using hollow fiber membranes: (a) profile of salt concentration across the membrane during OERO desalination process; (b) cross-section view and (c) front view of a hollow fiber bundle.

2.2. Calculating specific energy consumption

The specific energy consumption (E) is defined as an energy consumption per unit volume of product water, and it is related with the high-pressure pump, sweep low-pressure pump, and the energy recovery devices (ERDs) as presented in Fig. S2. The energy required for a regeneration step of sweep solution is not taken into consideration, because the diluted fertilizer sweep solution can be applied directly for irrigation. The calculation of E is thus given by [31],

$$E = \frac{P_f Q_f \left(\varepsilon_{pump}\right)^{-1} + P_{sw} Q_{sw} \left(\varepsilon_{pump}\right)^{-1} - P_b Q_b \varepsilon_{ERD}}{Q_P \times 3.6 \times 10^6} \tag{23}$$

Q_f and Q_b are the flow rates of feed and brine, respectively, P_f is the feed pressure, P_b is the outlet pressure, Q_P is the total permeated flow rate, P_{sw} is the inlet pressure of sweep solution,

Q_{sw} is the sweep flow rate, ε_{pump} is the efficiency of pressure pump and is assumed to be 0.85, ε_{ERD} is the efficiency of the energy recovery device and is assumed to be 0.95 [32].

2.3. Simulation algorithm

The system of equations is used to set up the mathematical model to evaluate the performance of the OERO process. **Fig. S1** presents the iteration algorithm for solving the mathematical model using MATLAB software (Mathworks, USA). The basic simulation conditions are listed in **Table 1**. Here, 0.6 M NaCl and 0.02 M NaCl were used as feed solution to simulate seawater and brackish water, respectively. Since the respective osmotic coefficients of KH_2PO_4 and NaCl are 0.85 and 0.93 [33-34] at 298 K, 0.6 M KH_2PO_4 and 0.02 M KH_2PO_4 were utilized as sweep solutions generating osmotic pressures of 25.3 bar and 0.84 bar, respectively, which are lower than that of 0.6 M NaCl (27.7 bar) and 0.02 M NaCl (0.92 bar) calculated by Eq. 3. The salt permeability (B) was set constant owing to the high salt rejection of RO membrane (typically > 99%) [35]. The fertilizer KH_2PO_4 was used as sweep solution, and its concentration is less than the concentration of feed solution.

Table 1. Specifications of the lab-made and commercial hollow fiber RO membrane modules

Element type	**Lab-made module for model verification**	**Commercial module for performance evaluation**
Module length (m)	0.32	0.68
Inner diameter (μm)	85	85
Outer diameter (μm)	175	175
No. of fibers	120	220000
Effective membrane area (m^2)	0.02	82.2
Distance between two fibers, f_d (μm)	200	53
Cross-section of module (m^2)	3.2×10^{-5}	0.01
Void fraction in the shell (ε)	0.886	0.458
Max. operating pressure (bar)	50	50
Pure water permeability ($L/(m^2.h.bar)$)	0.27	0.27
Salt permeability ($L/(m^2.h)$)	0.035	0.035
Structure parameter (μm)	1024	1024

3. Model verification

3.1. Materials and experimental methods

The commercial hollow fiber RO membranes used in the current study were obtained from TOYOBO Co. Ltd., Japan. The membranes were rinsed with deionized (DI) water and were kept in DI water prior to use. The detailed characteristics of the membranes are presented in **Table 1**.

To validate the model, the OERO performance was tested with a laboratory counter-flow HF module as shown in **Fig. 2**. Energy recovery device was not installed due to the limitations of the small laboratory-scale apparatus. The dimensions of the tubular channel were 320 mm length, 6.4 mm inner diameter and 9.7 mm outer diameter. A high pressure pump (P300, Wanner Pump Ltd.) and a variable speed gear pump (WT3000-1JA, Longer Precision Pump Co., Ltd.) were applied to pressurize the feed solution and to recirculate the sweep solution, respectively. The flow rate of both feed and sweep channels was kept constant at 0.1 L/h. The applied feed pressure was observed by using a digital pressure meter and was regulated through a backpressure valve at the outlet of the feed channel. The temperatures of both the feed and sweep solution were fixed at 25 ± 1 °C.

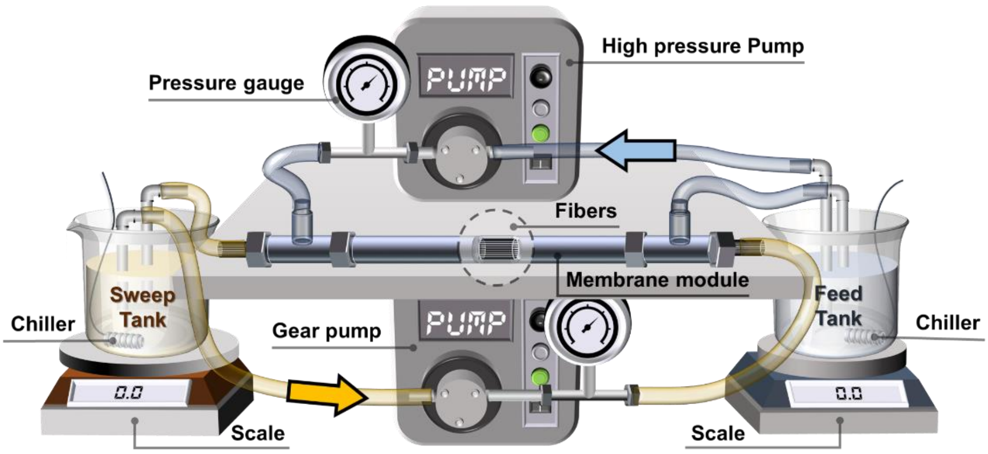

Fig. 2. Schematic diagram of the OERO performance evaluation system for the hollow fiber membranes.

3.2. Model verification

The simulated and experimental permeate fluxes as a function of the sweep concentration, the operating pressure at the module inlet, and the feed flow rate are shown in **Fig. 3**. The simulations demonstrate that the simulated water fluxes agree well with the experimental results. The average water flux increases logarithmically with the sweep concentration, indicating that the sweep solution is able to partially offset the osmotic pressure. As expected, a larger operating pressure results in a higher water flux (**Fig. 3b**) since OERO is a hydraulic pressure-driven process. Increasing feed flow rate would alleviate concentration polarization and thus enhance water flux (**Fig. 3c**). These results indicate that a better water recovery can be obtained in the presence of a high sweep solution, a suitable feed flow rate, and a comparatively large operating pressure. The model developed in this study is therefore an efficient tool to simulate filtration performance and optimize the OERO process.

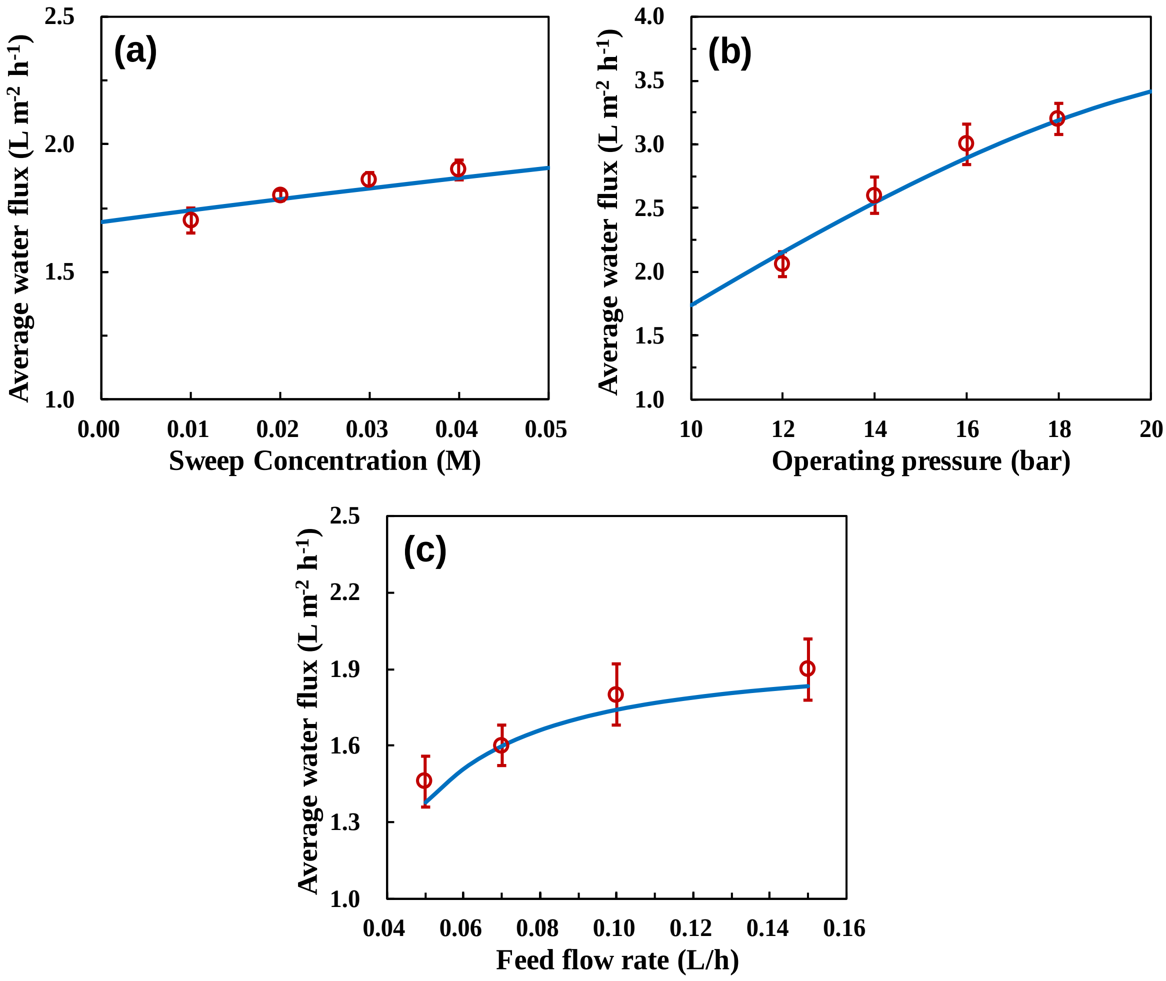

Fig. 3. Experimental (discrete symbols) and simulated (solid lines) water fluxes of lab-made HF RO membrane module as a function of (a) sweep concentration (constant operating pressure of 10 bar and constant feed flow rate of 0.1 L/h), (b) operating pressure (constant sweep concentration of 0.01 M KH_2PO_4 and constant feed flow rate of 0.1 L/h), and (c) feed flow rate (constant operating pressure of 10 bar and constant sweep concentration of 0.01 M KH_2PO_4). Experimental conditions: The feed solution fixed as 0.06 M NaCl and sweep flow rate fixed as 0.1 L/h.

4. Simulation results and discussion

4.1. Assessing the desalination performance under different membrane properties and geometry

The water transportation resistance across the membrane is affected by not only the membrane active layer but also the structure of the support layer due to existence of the internal concentration polarization (ICP) in the OERO process. The impacts of membrane properties including coefficient of water permeability (A) and parameter of support structure (S) on the water recovery for OERO system and conventional RO system are illustrated in **Fig. 4**. The water recovery in a conventional RO system is independent of the parameter of support structure. The recovery of OERO system is higher than that of conventional RO system especially in the case of seawater desalination, which is attributed to the greater osmotic pressure of the sweep solution (i.e., larger $\pi_{s,b}$ in eq. (1)). As shown in **Fig. 4a**, the recovery increases dramatically as the S decreases from 1500 to 500 μm when using 0.6 M KH_2PO_4 as sweep solution (SS) for treating high-salinity seawater owing to the decreased ICP modulus (i.e., smaller $\exp(-J_w S/D)$ in eq. (1)). Whereas only a minor enhancement is noticed when using a 0.1 M KH_2PO_4 as SS (**Fig. 4b**). It is attributed to the fact that the role of ICP in determining overall filtration resistance weakens with decreasing sweep concentration [36]. Thus, the recovery enhancement by decreasing the structure parameter is less effective under such conditions. Consistent with expectations, the influence of structure parameter on water recovery is negligible for the low-salinity brackish water when using lower KH_2PO_4 concentrations of 0.005 M and 0.02 M as SS (**Figs. 4c and d**). It is noteworthy that for both seawater and brackish water, the water recovery increases dramatically before eventually plateauing as the increase of water permeability coefficient. However, the influence of increasing *A* coefficient on the water recovery is more obvious in the case of brackish water reuse than that of seawater desalination. For instance, at *S* value of 1000 μm and 0.6 M KH_2PO_4 as SS (**Fig. 4a**), increasing *A* coefficient from 0.2 to 5.0 L m^{-2} h^{-1} bar^{-1} facilitates an increase of recovery from 33% to 51% (1.5 times) in the case of seawater desalination. In contrast, the water recovery exhibits a significant increase from 8% to 84% (10.5 times) in the case of brackish water reuse at *S* value of 1000 μm and 0.02 M KH_2PO_4 as SS (**Fig. 4c**). As a result, application of a more permeable membrane in OERO process offers a high water recovery for brackish water reuse, but the efforts to increase water recovery for seawater desalination should focus on decreasing the structure parameter of membrane.

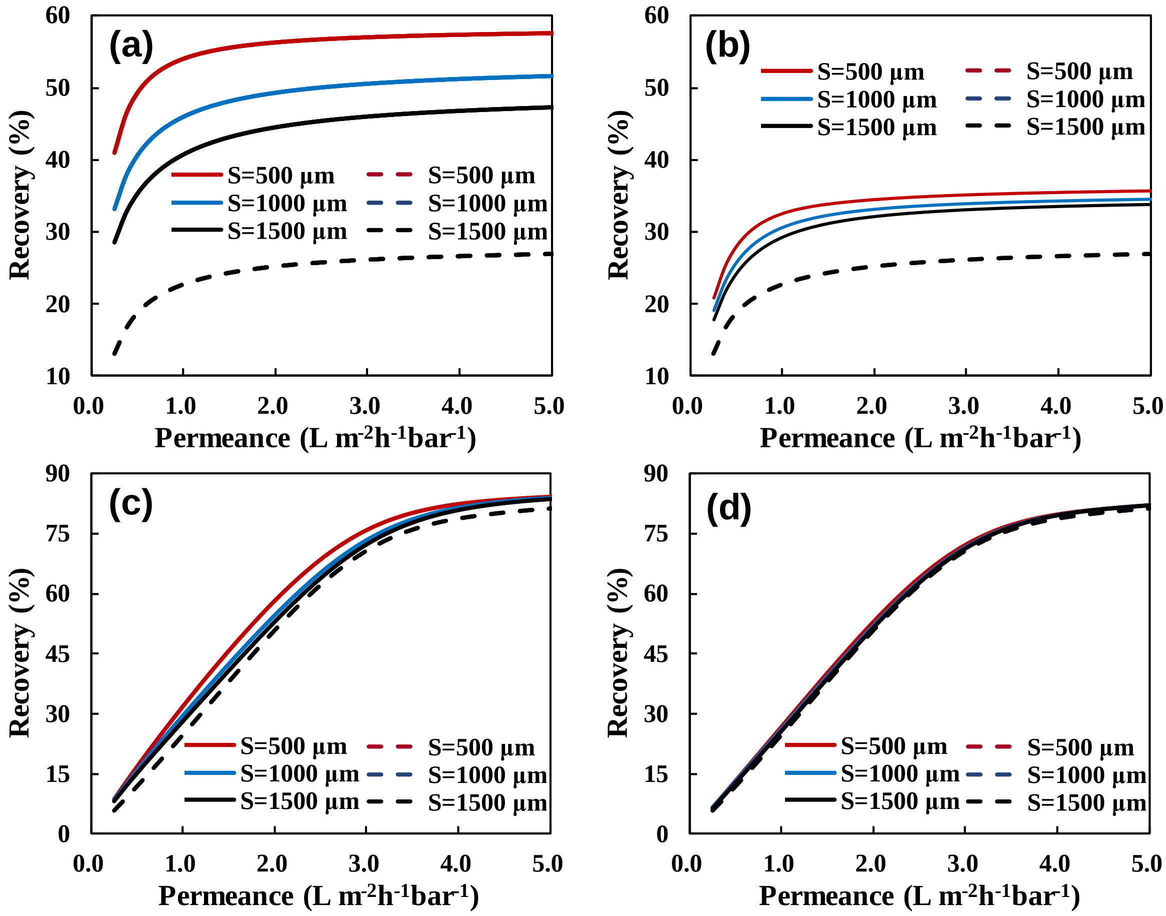

Fig. 4. Simulated water recovery of commercial HF RO membrane module with varied membrane water permeance and support structure parameter (*S*) in OERO system (solid line) and conventional RO system (dash line). Simulation conditions for OERO system: both the

feed and sweep flow rates were fixed at 1 m^3/h. (a) 0.6 M NaCl as feed solution (FS), 0.6 M KH_2PO_4 as sweep solution (SS), and operating pressure of 40 bar; (b) 0.6 M NaCl as FS, 0.1 M KH_2PO_4 as SS, and operating pressure of 40 bar; (c) 0.02 M NaCl as FS, 0.02 M KH_2PO_4 as SS, and operating pressure of 7 bar; (d) 0.02 M NaCl as FS, 0.005 M KH_2PO_4 as SS, and operating pressure of 7 bar. Simulation conditions for conventional RO system are the same as that of the OERO system, in which the sweep solutions are not included.

Fiber geometry is particularly effective for avoiding the severe concentration and dilution effects through optimizing hydraulic environments in the OERO process [37]. The simulation results for investigating the effects of the fiber diameter and length on water recovery and energy consumption are demonstrated in **Fig. 5**. In both cases of seawater desalination and brackish water reuse, the water recovery increases monotonically with increasing fiber length (**Figs. 5a-b**). The increase can be attributed to the increased total membrane area resulting in larger permeate volume. The energy consumption decreases first and then gradually reaches a plateau with increasing fiber length in both cases (**Figs. 5a-b**). The decrease can be attributed to the increased water recovery with the increase of fiber length. However, further increasing fiber length results in greater pressure drops in the shell (P_S) and thus less channel pressure at the outlet (P_b), which implies a decrease of energy recovery by the EDRs (i.e., smaller $P_b Q_b \varepsilon_{ERD}$ in eq. (23)).

In contrast, a monotonic decrease in water recovery with increasing fiber diameter is observed in both cases of high-salinity seawater desalination and low-salinity brackish water reuse (**Figs. 5c-d**). The reason is that increasing fiber diameter reduces the packing density, thereby decreasing the effective filtration area [38]. As a result, a monotonic reduction of the water recovery is observed in both cases. The energy consumption decreases monotonically with increasing fiber diameter in the case of seawater desalination (**Fig. 5c**). However, for the brackish water reuse, the energy consumption decreases first and then increases with increasing fiber diameter. This interesting phenomenon is attributed to two competing factors. One is that increasing fiber diameter decreases pressure drop [39], and thus a decreased energy consumption is observed in the case of brackish water reuse. The other is that the enhancement of fiber diameter reduces the effective filtration area, and thus further increasing fiber diameter would decrease water production efficiency. However, for high-salinity seawater, an extremely high hydraulic pressure is used to offset the high osmotic pressure, and thereby the effect of decreased pressure drop on overall energy consumption is significant. As a result, a monotonic reduction of the energy consumption is observed in the case of seawater desalination.

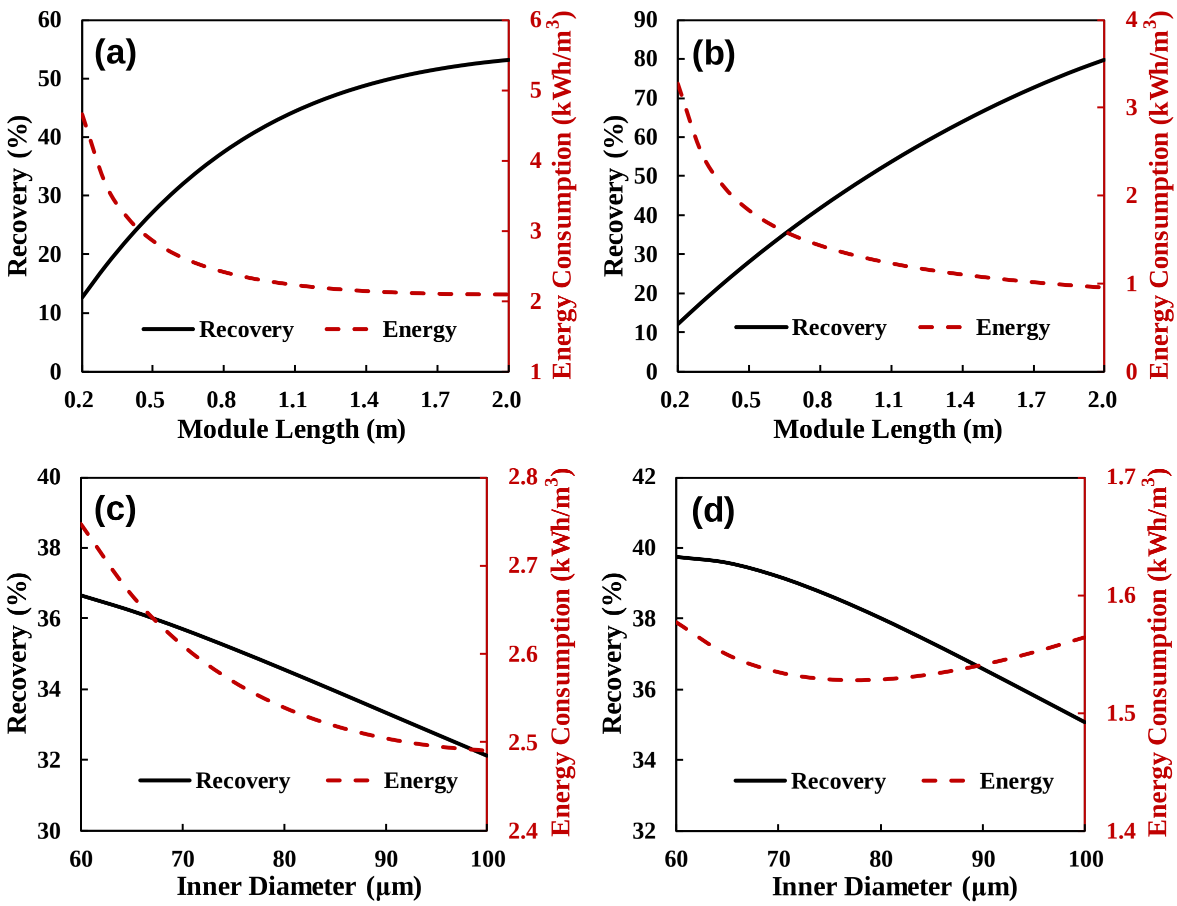

Fig. 5. Simulated water recovery and specific energy consumption of commercial HF RO membrane module with varied (a-b) module length and (c-d) fiber inner diameter. Simulation conditions: number density of fibers in the cross-section of module varied with fiber diameter since distance between two fibers fixed as 53 μm; both the feed and sweep flow rates fixed as 1 m^3/h. (a, c) 0.6 M NaCl as FS, 0.6 M KH_2PO_4 as SS, and operating pressure of 40 bar; (b, d) 0.02 M NaCl as FS, 0.02 M KH_2PO_4 as SS, and operating pressure of 20 bar.

To further reveal the intrinsic relationship between the fiber geometry and water production efficiency, the water recovery and energy consumption are plotted against both the fiber length and diameter as shown in **Fig. 6**. In both cases, when the fiber diameter is fixed the water recovery increased monotonously with enhancing fiber length (**Figs. 6a and c**). Thus, the energy consumption decreased as increasing fiber length with any fiber diameter in the case of brackish water reuse (**Fig. 6d**). However, for the case of seawater desalination, the energy consumption first decreased and then increased with enhancing fiber length especially as the fiber diameter is less than 70 μm, indicating the existence of optimum fiber length (**Fig. 6b**). Therefore, energy consumption is mainly dependent on fiber diameter and fiber length for high-salinity seawater and low-salinity brackish water, respectively (**Figs. 6b and d**). There exists a trade-off and economic optimum fiber geometry by balancing the energy and recovery. It may be necessary to choose relatively longer fibers for achieving highly efficient brackish water reuse. Whereas, in the case of seawater desalination, larger diameter fibers are preferred.

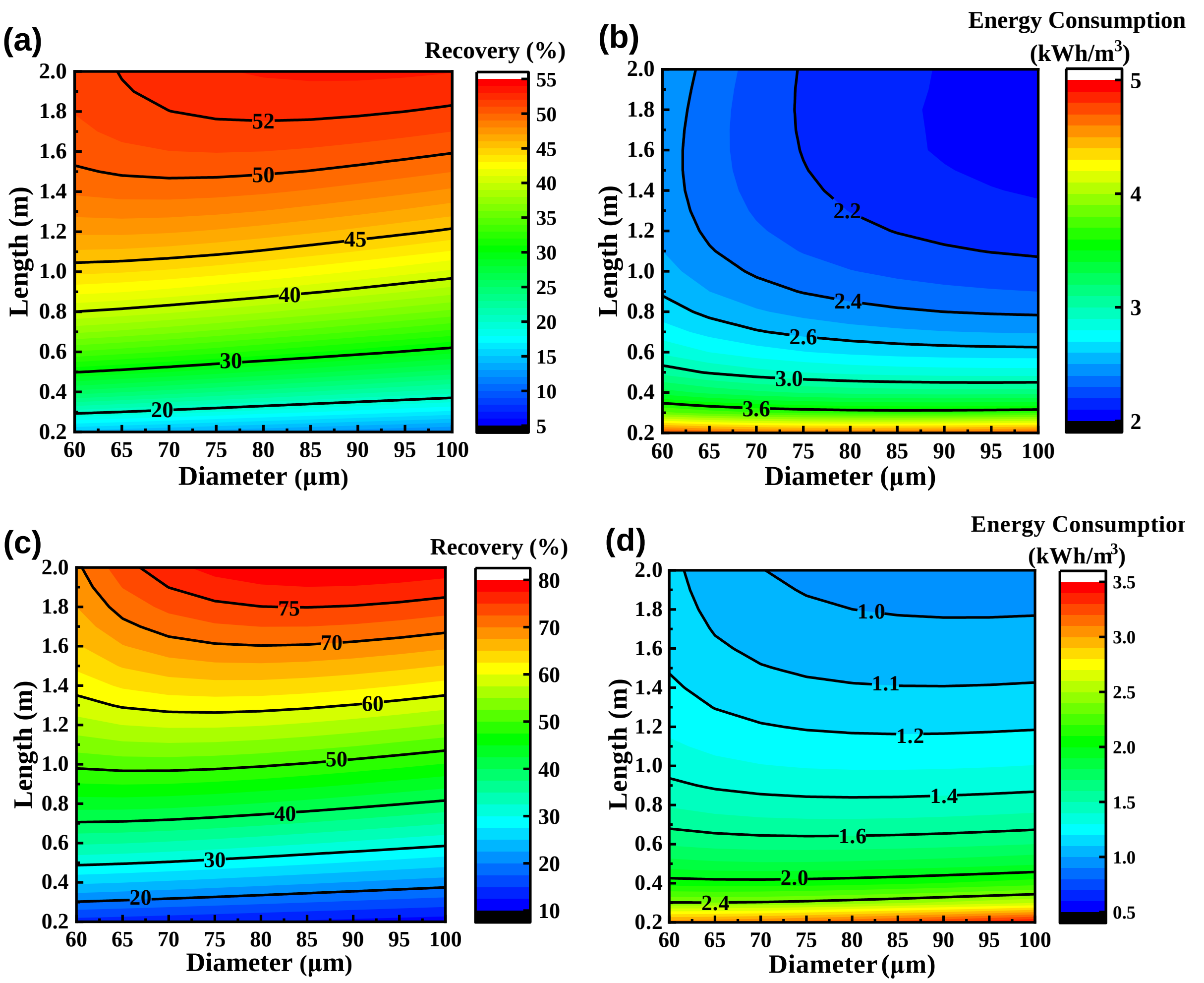

Fig. 6. Simulated (a, c) water recovery and (b, d) specific energy consumption of commercial HF RO membrane module with varied module length and fiber inner diameter for seawater and brackish water. Simulation conditions: number density of fibers in the cross-section of module varied with fiber diameter since distance between two fibers fixed as 53 μm; both the feed and sweep flow rates fixed as 1 m^3/h. (a-b) 0.6 M NaCl as FS, 0.6 M KH_2PO_4 as SS, and operating pressure of 40 bar; (c-d) 0.02 M NaCl as FS, 0.02 M KH_2PO_4 as SS, and operating pressure of 20 bar.

4.2. Assessing the desalination performance under different process parameters

In this section, we systematically investigate the impacts of operating parameters including sweep concentration, flow rate, and operating pressure on the filtration performance of the OERO process, and elaborate their inherent relationships (**Figs. 7 and 8**).

In both cases, the water recovery increased monotonically with increasing sweep concentration (**Figs. 7a-b**) owing to the higher driving force resulting from increasable osmotic pressure of the sweep solution (i.e., larger $\pi_{s,b}$ in eq. (1)). The enhanced water recovery results in the decrease of energy consumption (**Figs. 7a-b**). Increasing sweep flow rate would alleviate concentration polarization, resulting in an increase of water recovery (**Fig. 7c**). However, higher sweep flow rate also results in an enhancement of the pressure drop in the pore side (i.e., larger P_i in eq. (4)), indicating a lower effective hydraulic pressure. Meanwhile, compared to the high-salinity seawater desalination, the concentration polarization degree is less in the reuse of low-salinity brackish water because of the low sweep concentration. As a result, the sweep flow rate influencing on the water recovery is not significant in the case of brackish water reuse (**Fig. 7d**). In addition, increasing sweep flow rate leads to a dramatic increase in the energy consumption for both cases because of the increased power consumption by the sweep low-pressure pump (i.e., larger $P_{sw}Q_{sw}\left(\varepsilon_{pump}\right)^{-1}$ in eq. (23)) (**Figs. 7c-d**).

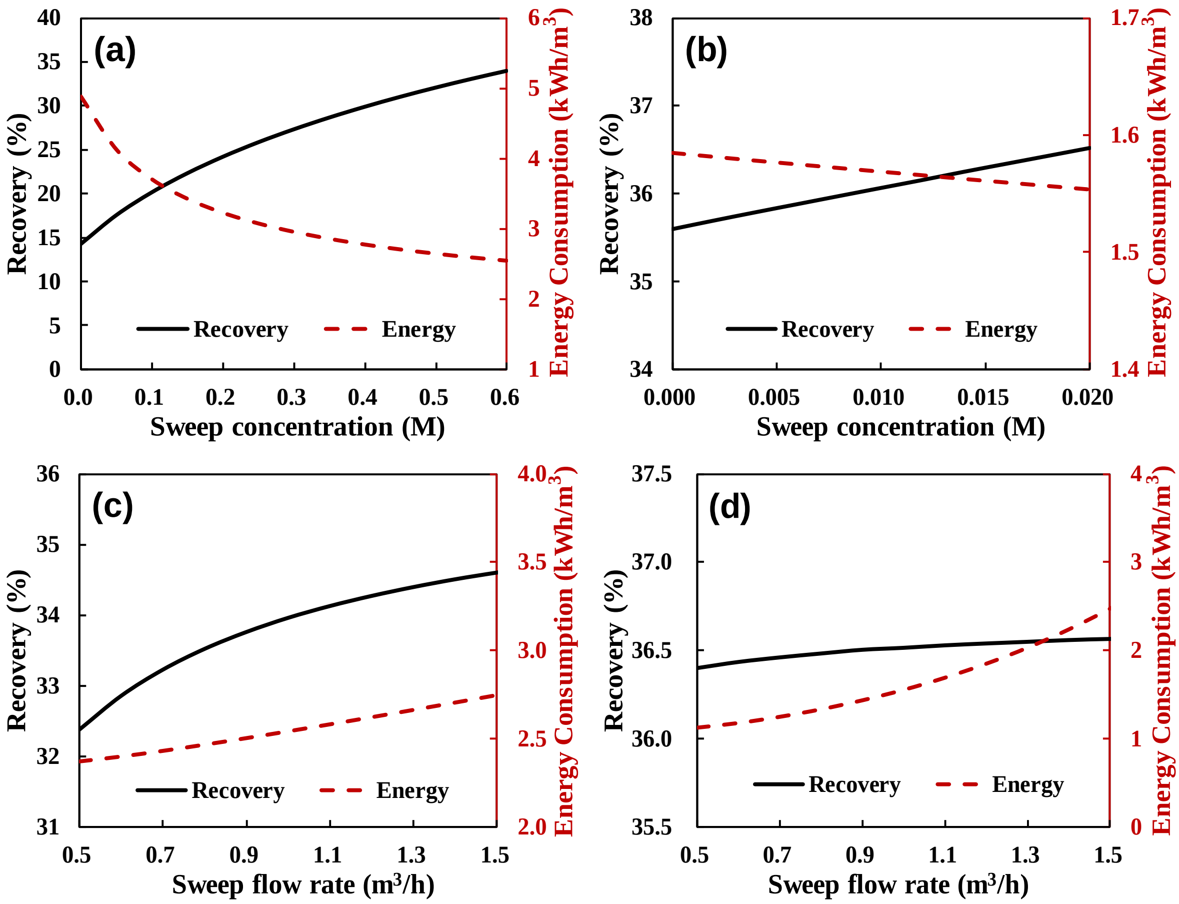

Fig. 7. Simulated water recovery and specific energy consumption of commercial HF RO membrane module with varied (a-b) sweep concentration and (c-d) sweep flow rate. Simulation conditions: feed flow rate fixed as 1 m^3/h. Sweep flow rate fixed as (a-b) 1 m^3/h; FS fixed as (a and c) 0.6 M NaCl and (b and d) 0.02 M NaCl, respectively; operating pressure fixed as (a and c) 40 bar and (b and d) 20 bar, respectively; SS fixed as (c) 0.6 M KH_2PO_4 and (d) 0.02 M KH_2PO_4, respectively.

Fig. 8 presents the effects of feed flow rate and operating pressure on the water recovery and specific energy consumption. In both cases, decreasing feed flow rate significantly increases the water recovery and decreases the energy consumption, indicating that a suitable flow rate is of significant importance for realizing efficient desalination (**Figs. 8a-b**). The decreased energy consumption at the lower feed flow rate is attributed to the decreased power consumption by the feed high-pressure pump (i.e., smaller $P_f Q_f \left(\varepsilon_{pump}\right)^{-1}$ in eq. (23)) and the lower pressure drop in the shell (i.e., smaller P_S in eq. (5)). Notably, when the feed flow rate decreased to 0.5 m^3/h, the energy consumption of high-salinity seawater desalination decreased to 2.2 kWh/m^3, which is lower than 3 kWh/m^3 (that is the current energy consumption level of the conventional seawater RO desalination [1]). It further confirms that the OERO system is more efficient than the conventional RO system. In both cases, **Figs. 8c-d** present that increasing operating pressure enhances the water recovery linearly. This is attributed to the enhanced water flux at higher hydraulic pressure (**Figs. S3a-b**). The assessment of concentration polarization demonstrated that ICP provides the dominated resistance to mass transfer in typical OERO operation, which becomes more severe with the increase of operating pressure (**Figs. S3c-d**). Compared to the seawater desalination mode at the operating pressure of 40 bar, the water recovery of the brackish water desalination mode exhibited higher water recovery and lower energy consumption at the elevated operating pressure (>20 bar). The increased water recovery contributes to the decreased energy consumption. However, with further increase in operating pressure, the energy consumption gradually approaches a minimum value in the case of brackish water reuse (**Fig. 8d**) whereas it decreases first then increases in the case of seawater desalination (**Fig. 8c**). These results are attributed to the fact that the increased operating pressure results in a drastic enhancement in the power consumption by a high-pressure pump (i.e., larger $P_f Q_f \left(\varepsilon_{pump}\right)^{-1}$ in eq. (23)) especially when a high hydraulic pressure is applied as in the seawater desalination. An optimal operating pressure exists for high-salinity seawater to achieve highly efficient water production when other operating conditions are fixed.

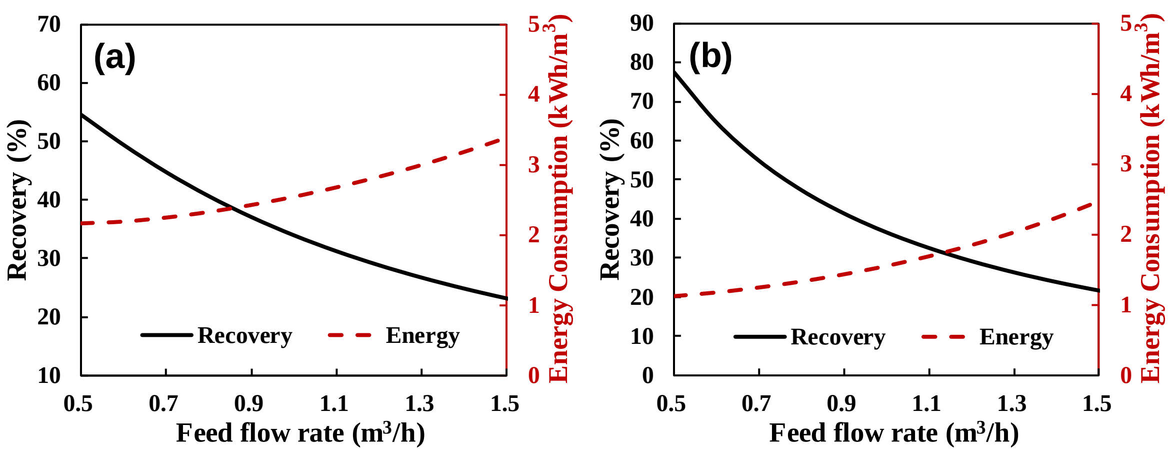

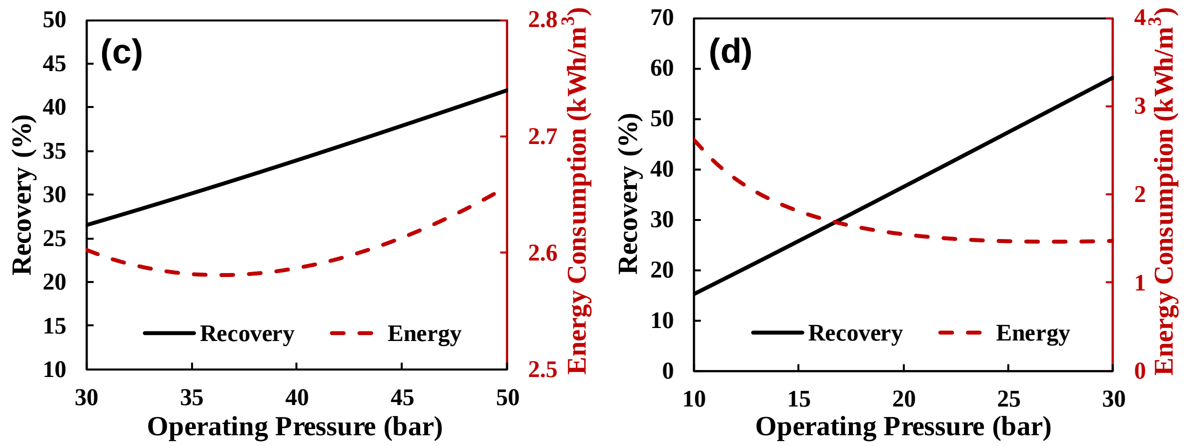

Fig. 8. Simulated water recovery and specific energy consumption of commercial HF RO membrane module with varied (a-b) feed flow rate and (c-d) operating pressure. Simulation conditions: sweep flow rate fixed as 1 m^3/h. Operating pressure fixed as (a) 40 bar and (b) 20 bar, respectively; feed flow rate fixed as (c-d) 1 m^3/h; FS fixed as (a and c) 0.6 M NaCl and (b and d) 0.02 M NaCl, respectively; SS fixed as (a and c) 0.6 M KH_2PO_4 and (b and d) 0.02 M KH_2PO_4, respectively.

5. Implications

The OERO process has been proven to be a feasible alternative for the desalination of saline water with a higher water recovery at a lower operating pressure [8]. To address the challenges of separation of low-concentration sweep solution from desalinated water for recycle, a usable sweep solution can be used where appropriate. For example, a fertilizer solution can be applied as sweep solution so that the permeate solutions can be directly used for fertilized irrigation. Such an approach not only decreases the energy consumption of the OERO process, but also achieves a near-zero liquid discharge especially for low-salinity feed water. Although the concept of fertilizer drawn desalination has been suggested in the forward osmosis process, the development is constrained by severe reverse solute flux and the requirement of further dilution of the produced draw solution to meet the standard of fertigation due to the limitation of osmotic equilibrium [14]. In the OERO system, the reverse solute diffusion is less severe or even negligible [7]. The generated diluted fertilizer permeation is potentially suitable for direct fertigation especially in the conditions of high applied pressure and low concentration of sweep solution. For instance, the final diluted sweep solution is 0.18 g/L KH_2PO_4 in the case of brackish water reuse (P_f =20 bar, Q_f/Q_{sw}=10, $C_{s,b}$=0.005 M), which is below the tolerable phosphate concentration of 194 mg/L for a drip irrigation system [40]. In addition, as supreme allowable hydraulic pressure of RO membrane is fixed, OERO process can be carried out within a range of water recovery where the conventional RO technology cannot tolerate (**Fig. 9**). Our study has also revealed that a higher water recovery (up to 90%) can be achieved by using a high permeability membrane, high sweep concentration and operating pressure in the case of brackish water reuse. Hence, OERO process shows great promise to break through the limit of conventional RO technology in desalination field.

Furthermore, the OERO system can alternatively be incorporated into the conventional multi-stage RO process. A previous study demonstrated that use of one or more permeable nanofiltration (NF) stages in connection to RO stages in series could increase overall water recovery and reduce energy consumption [32]. However, the combined NF-RO process is limited by the high solute permeability of the NF membrane, which would impact the quality of permeation. The OERO system may replace the NF stage to connect the RO stages for simultaneously supplying potable water and fertilized irrigation (**Fig. S4**). This combined OERO-RO system may be attractive in the water-scarce islands and inlands where agricultural activities are important to their economy.

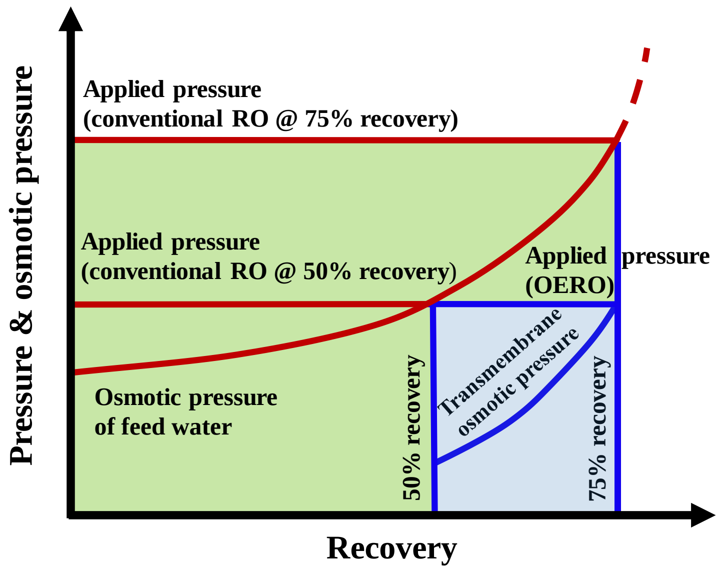

Fig. 9. Comparison of the pressure as a function of water recovery in the conventional RO and the OERO systems.

This study also presents us a conspicuous feasibility of hollow fiber membrane for the OERO process in terms of high water recovery and low energy consumption. Nevertheless, there is still much room for further improvement of the hollow fiber membrane. By increasing the water permeance to 5.0 L/m^2 h bar, the water productivity can achieve a 10-fold enhancement for low-salinity brackish water reuse (**Fig. 4c**). Reducing the thickness of the membrane support to 500 μm also leads to a 50% enhancement in the water productivity for high-salinity seawater (**Fig. 4a**). However, decrease of the fiber structure parameter will lead to the decrease of its mechanical strength. To address this issue, braid-reinforced hollow fiber membrane could be fabricated to strengthen the membrane mechanical stability without reducing the structure parameter [41]. In addition, membrane fouling is a pervasive problem for all membrane processes. Especially the combined organic fouling and mineral scaling is a key issue for treating high-salinity shale gas wastewaters [8]. Development of membranes with antifouling properties are of special importance to achieve a more sustainable OERO process in such applications. On the other hand, the tailoring of the sweep solution chemistry may further allow the proper control of fouling and scaling of the RO membrane [42]. An enhancement in flow rate alleviates concentration polarization, thereby mitigating fouling in OERO. However, further increasing flow rate leads to a decrease in module efficiency (**Figs. 8a-b**) due to an increase in pressure drop and a reduction in water recovery [21]. This indicates that an optimal flow rate is needed to realize an efficient operation. For the purpose of fouling control, increasing flow rate can be potentially done intermittently to reverse some of the fouling. Alternatively, operating in transient cycles/batches could be potentially adopted. Nevertheless, further research is needed to verify the effectiveness of these approaches for OERO. In summary, future studies should be focused on the optimization of the OERO system on the basis of economic assessments, and development of high-performance RO membranes (i.e., with low structure parameter, high water permeability, and antifouling properties, etc.).

6. Conclusion

By establishing a mathematical model of a hollow fiber membrane module, we demonstrated that the OERO unit with an appropriate sweep solution can achieve a higher water recovery in treating both high-salinity seawater and low-salinity brackish water, than the conventional RO process. The results indicate that the enhancement in water recovery can be achieved by the decrease of the fiber structure parameter for high-salinity seawater, and by the increase of the membrane permeance for low-salinity brackish water. Our examination of the fiber geometry influence on water recovery revealed that longer fibers are preferable for low-salinity brackish water, while fibers with larger diameters are more suitable for high-salinity seawater. In addition, the water production efficiency can be enhanced by increasing the sweep concentration and the operating pressure. A higher flow rate of the sweep solution can effectively reduce the concentration polarization in the treatment of high-salinity seawater. The simulation results are supported by experimental studies. Our work provides theoretical perspectives for understanding the performance of hollow fiber membrane modules in OERO plants and highlights the promise of the use of fertilizer as sweep solution in the OERO process for “near zero discharge desalination”.

Acknowledgements

The study is supported by the Research Grants Council of the Hong Kong Special Administration Region (C7051-17G), and is partially supported by the Program for Guangdong Introducing Innovative and Entrepreneurial Teams (2019ZT08L213) and Key Special Project for Introduced Talents Team of Southern Marine Science and Engineering Guangdong Laboratory (Guangzhou) (GML2019ZD0403).

List of Symbols

Latin symbols

A	permeability coefficient of water (m s^{-1} bar^{-1})
A_{fiber}	occupied area of each fiber (m^2)
A_{flow}	the cross sectional flow area in the fiber lumen (m^2)

$A_{hexagon}$	catchment area of each fiber (m^2)
B	permeability coefficient of salt ($m\ s^{-1}$)
C	concentration of solute ($mol\ L^{-1}$)
$C_{f,b}$	feed concentration ($mol\ L^{-1}$)
$C_{s,b}$	sweep concentration ($mol\ L^{-1}$)
D	diffusion coefficient of salt ($m^2\ s^{-1}$)
d_h	hydraulic diameter (m)
d_i	inner diameter of the fiber (m)
d_o	outer diameter of the fiber (m)
d_p	characteristic diameter (m)
E	specific energy consumption ($kWh\ m^{-3}$)
f_d	distance between two fibers (m)
I	number of dissociating species (-)
J_s	salt flux ($m^3\ m^{-2}\ s^{-1}$)
J_w	water flux ($m^3\ m^{-2}\ s^{-1}$)
k	feed salt mass transfer coefficient ($m\ s^{-1}$)
l_{mem}	fiber length (m)
P_b	channel pressure at the outlet (bar)
P_i	pressure drop in the pore side (bar)
P_f	feed pressure (bar)
P_{fiber}	perimeter of circular cross section of the fiber
P_{sw}	inlet pressure of sweep solution (bar)
P_S	pressure drop in the shell (bar)
Q_b	brine flow rate at the outlet ($m^3\ s^{-1}$)
Q_f	feed flow rate at the inlet ($m^3\ s^{-1}$)
Q_P	total permeated flow rate ($m^3\ s^{-1}$)
Q_{sw}	sweep flow rate ($m^3\ s^{-1}$)
R	gas constant ($L\ bar\ mol^{-1}\ K^{-1}$)
R_e	Reynolds number (-)
S	structure parameter of the membrane (m)

S_c Schmidt number (-)

S_h Sherwood number (-)

S_{h1} parameter used for determining Sherwood number (-)

S_{h2} parameter used for determining Sherwood number (-)

S_{h3} parameter used for determining Sherwood number (-)

T temperature (K)

Greek Letters

ΔP applied hydraulic pressure (bar)

ε void fraction of the module (-)

ε_{ERD} energy recovery device efficiency (-)

ε_{pump} high pressure pump efficiency (-)

μ feed viscosity (Pa s)

$\pi_{f,b}$ feed osmotic pressure (bar)

$\pi_{s,b}$ sweep osmotic pressure (bar)

ρ liquid density (kg/m^3)

v flow velocity (m s^{-1})

v_i flow velocity in the pore side (m s^{-1})

v_s flow velocity in the shell (m s^{-1})

Subscripts

NaCl NaCl salt solution

KH2PO4 KH_2PO_4 salt solution

References

[1] M. Elimelech, W.A. Phillip, The future of seawater desalination: energy, technology, and the environment, Science 333 (2011) 712-717.

[2] L.F. Greenlee, D.F. Lawler, B.D. Freeman, B. Marrot, P. Moulin, Reverse osmosis desalination: Water sources, technology, and today's challenges, Water Res. 43 (2009) 2317-2348.

[3] C.Y. Tang, Z. Yang, H. Guo, J.J. Wen, L.D. Nghiem, E. Cornelissen, Potable Water Reuse through Advanced Membrane Technology, Environ. Sci. Technol. 52(18) (2018) 10215-10223.

[4] X. Li, D. Hasson, R. Semiat, H. Shemer, Intermediate concentrate demineralization techniques for enhanced brackish water reverse osmosis water recovery-A review, Desalination 466 (2019) 24-35.

[5] J.R. Werber, A. Deshmukh, M. Elimelech, The critical need for increased selectivity, not increased water permeability, for desalination membranes, Environ. Sci. Technol. Lett. 3 (2016) 112-120.

[6] X. Chen, N.Y. Yip, Unlocking high-salinity desalination with cascading osmotically mediated reverse osmosis: energy and operating pressure analysis, Environ. Sci. Technol. 52 (2018) 2242-2250.

[7] J. Kim, D.I. Kim, S. Hong, Analysis of an osmotically-enhanced dewatering process for the treatment of highly saline (waste) waters, J. Membr. Sci. 548 (2018) 685-693.

[8] C.D. Peters, N.P. Hankins, Osmotically assisted reverse osmosis (OARO): Five approaches to dewatering saline brines using pressure-driven membrane processes, Desalination 458 (2019) 1-13.

[9] J. Kim, J. Kim, J. Kim, S. Hong, Osmotically enhanced dewatering-reverse osmosis (OED-RO) hybrid system: implications for shale gas produced water treatment, J. Membr. Sci. 554 (2018) 282-290.

[10] T.V. Bartholomew, L. Mey, J.T. Arena, N.S. Siefert, M.S. Mauter, Osmotically assisted reverse osmosis for high salinity brine treatment, Desalination 421 (2017) 3-11.

[11] C.D. Peters, N.P. Hankins, The synergy between osmotically assisted reverse osmosis (OARO) and the use of thermo-responsive draw solutions for energy efficient, zero-liquid discharge desalination, Desalination 493 (2020) 114630.

[12] L. Chekli, Y. Kim, S. Phuntsho, S. Li, N. Ghaffour, T. Leiknes, H.K. Shon, Evaluation of fertilizer-drawn forward osmosis for sustainable agriculture and water reuse in arid regions, J. Environ. Manage. 187 (2017) 137-145.

[13] M. Xie, M. Zheng, P. Cooper, W.E. Price, L.D. Nghiem, M. Elimelech, Osmotic dilution for sustainable green wall irrigation by liquid fertilizer: Performance and implications, J.

Membr. Sci. 494 (2015) 32-38.

[14] S. Phuntsho, H.K. Shon, S. Hong, S. Lee, S. Vigneswaran, A novel low energy fertilizer driven forward osmosis desalination for direct fertigation: Evaluating the performance of fertilizer draw solutions, J. Membr. Sci. 375 (2011) 172-181.

[15] Y.C. Kim, M. Elimelech, Adverse Impact of Feed Channel Spacers on the Performance of Pressure Retarded Osmosis, Environ. Sci. Technol. 46 (2012) 4673-4681.

[16] C. Lee, J. Jang, N.T. Tin, S. Kim, C.Y. Tang, I.S. Kim, Effect of spacer configuration on the characteristics of FO membranes: Alteration of permeation characteristics by membrane deformation and concentration polarization, Environ. Sci. Technol. 54(10) (2020) 6385-6395.

[17] Q.H. She, D.X. Hou, J.X. Liu, K.H. Tan, C.Y. Tang, Effect of feed spacer induced membrane deformation on the performance of pressure retarded osmosis (PRO): Implications for PRO process operation, J. Membr. Sci. 445 (2013) 170-182.

[18] W. Gai, D.L. Zhao, T.S. Chung, Thin film nanocomposite hollow fiber membranes comprising Naþfunctionalized carbon quantum dots for brackish water desalination, Water Res. 154 (2019) 54-61.

[19] Y. Tanaka, M. Yasukawa, S. Goda, H. Sakurai, M. Shibuya, T. Takahashi, M. Kishimoto, M Higa, H. Matsuyama, Experimental and simulation studies of two types of 5-inch scale hollow fiber membrane modules for pressure-retarded osmosis, Desalination 447 (2018) 133-146.

[20] D. Attarde, M. Jain, P.K. Singh, S.K. Gupta, Energy-efficient seawater desalination and wastewater treatment using osmotically driven membrane processes, Desalination 413 (2017) 86-100.

[21] N. Togo, K. Nakagawa, T. Shintani, T. Yoshioka, T. Takahashi, E. Kamio, H. Matsuyama, Osmotically assisted reverse osmosis utilizing hollow fiber membrane module for concentration process, Ind. Eng. Chem. Res. 58 (2019) 6721-6729.

[22] M. Askari, C.Z. Liang, L.T. Choong, T.S. Chung, Optimization of TFC-PES hollow fiber membranes for reverse osmosis (RO) and osmotically assisted reverse osmosis (OARO) applications, J. Membr. Sci. 625 (2021) 119156.

[23] W.X. Fang, R. Wang, S.R. Chou, L. Setiawan, A.G. Fane, Composite forward osmosis

hollow fiber membranes: Integration of RO- and NF-like selective layers to enhance membrane properties of anti-scaling and anti-internal concentration polarization, J. Membr. Sci. 394-395 (2012) 140-150.

[24] M. Sekino, Study of an analytical model for hollow fiber reverse osmosis module systems, Desalination 100 (1995) 85-97.

[25] M. Shibuya, M. Yasukawa, S. Goda, H. Sakurai, T. Takahashi, M. Higa, H. Matsuyama, Experimental and theoretical study of a forward osmosis hollow fiber membrane module with a cross-wound configuration, J. Membr. Sci. 504 (2016) 10-19.

[26] F. Lipnizki, R.W. Field, Mass transfer performance for hollow fibre modules with shell-side axial feed flow: using an engineering approach to develop a framework, J. Membr. Sci. 193 (2001) 195-208.

[27] V. Vitagliano, P.A. Lyons, Diffusion coefficients for aqueous solutions of sodium chloride and barium chloride, J. Am. Chem. Soc. 78 (1956) 1549-1552.

[28] H.L. Zhang, S.J. Han, Viscosity and density of water + sodium chloride + potassium chloride solutions at 298.15 K, J. Chem. Eng. Data 41 (1996) 516-520.

[29] F. Chenlo, R. Moreira, G. Pereira, M.J. Vázquez, Viscosity of binary and ternary aqueous systems of NaH2PO4, Na2HPO4, Na3PO4, KH2PO4, K2HPO4, and K3PO4, J. Chem. Eng. Data 41 (1996) 906-909.

[30] J.D. Hatfield, O.W. Edwards, R.L. Dunn, Diffusion coefficients of aqueous solutions of ammonium and potassium orthophosphates at 25o, J. Phys. Chem. 70 (1966) 2555-2561.

[31] D.C. Tanugi, R.K. McGovern, S.H Dave, J.H. Lienhard, J.C. Grossman, Quantifying the potential of ultra-permeable membranes for water desalination, Energ. Environ. Sci. 7 (2014) 1134-1141.

[32] A. Zhu, P.D. Christofides, Y. Cohen, Energy consumption optimization of reverse osmosis membrane water desalination subject to feed salinity fluctuation, Ind. Eng. Chem. Res. 48(21) (2009) 9581-9589.

[33] R.F.G.J. King, B. Jones, J.P. O'Hara, The availability of water associated with glycogen during dehydration: a reservoir or raindrop? Eur. J. Appl. Physiol. 118 (2018) 283-290.

[34] J.H. Oh, A. Jang, Application of chlorine dioxide (ClO_2) to reverse osmosis (RO)

membrane for seawater desalination, J. Taiwan Inst. Chem. Eng. 68 (2016) 281-288.
[35] Z. Yang, H. Guo, C.Y. Tang, The upper bound of thin-film composite (TFC) polyamide membranes for desalination, J. Membr. Sci. 590 (2019) 117297.
[36] C.Y. Tang, Q. She, W.C.L. Lay, R. Wang, R. Field, A.G. Fane, Modeling double-skinned FO membranes, Desalination 283 (2011) 178-186.
[37] D. Xiao, W. Li, S. Chou, R. Wang, C.Y. Tang, A modeling investigation on optimizing the design of forward osmosis hollow fiber modules, J. Membr. Sci. 392-393 (2012) 76-87.
[38] M.G. Ahunbay, S.B. Tantekin-Ersolmaz, W.B. Krantz, Energy optimization of a multistage reverse osmosis process for seawater desalination, Desalination 429 (2018) 1-11.
[39] X. Li, J. Li, H. Wang, X. Huang, B. He, Y. Yao, J. Wang, H. Zhang, H.H. Ngo, W. S. Guo, A filtration model for prediction of local flux distribution and optimization of submerged hollow fiber membrane module, AIChE J. 61(12) (2015) 4377-4386.
[40] S. Phuntsho, H.K. Shon, T. Majeed, I. El Salibya, S. Vigneswarana, J. Kandasamy, S. Hong, S. Lee, Blended fertilisers as draw solutions for fertilizer-drawn forward osmosis desalination, Environ. Sci. Technol. 46 (2012) 4567-4575.
[41] L. Xia, J. Ren, J.R. McCutcheon, Braid-reinforced thin film composite hollow fiber nanofiltration membranes, J. Membr. Sci. 585 (2019) 109-114.
[42] M. Zhang, Q. She, X. Yan, C.Y. Tang, Effect of reverse solute diffusion on scaling in forward osmosis: A new control strategy by tailoring draw solution chemistry, Desalination 401(2017) 230-237.